Nanoscale

PAPER

View Article Online
View Journal

Cite this: DOI: 10.1039/d5nr05112f

Influence of microenvironmental viscosity on the cellular uptake of Fe_3O_4 nanoparticles and their anticancer effect

Man Wang, [a,b] Huajian Chen,[a] Rui Sun,[a] Tianjiao Zeng, [a,b] Chengyu Lu,[a,b] Toru Yoshitomi, [a] Naoki Kawazoe,[a] Yingnan Yang[c] and Guoping Chen *[a,b]

Received 4th December 2025,
Accepted 8th April 2026

DOI: 10.1039/d5nr05112f

rsc.li/nanoscale

Viscosity is a characteristic property of extracellular microenvironments, and it varies among cancer tissues. Although internalized magnetic nanoparticles are crucial for magnetic hyperthermia, the influence of microenvironmental viscosity on their cellular uptake remains elusive. In this study, the effect of microenvironmental viscosity on the cellular uptake of magnetic nanoparticles and the efficiency of magnetic hyperthermia were investigated by culturing colorectal cancer cells in media of different viscosities. Results showed that the cellular uptake of magnetic nanoparticles significantly decreased with increasing microenvironmental viscosity, which further decreased the intracellular heating effect of magnetic nanoparticles. Furthermore, the proportion of apoptotic cells induced by magnetic hyperthermia was significantly reduced in high viscosity microenvironments, and the most viscous microenvironment exhibited the lowest apoptosis rate. This study revealed the important role of microenvironmental viscosity in regulating the cellular uptake of magnetic nanoparticles and the efficiency of magnetic hyperthermia, which provides a novel perspective for optimizing the application of magnetic hyperthermia in anticancer therapy.

1. Introduction

Nanomaterials have been extensively investigated and used in biomedical applications because of their unique properties such as small size, large specific surface area and high penetration capacity.[1–3] Accordingly, nanomaterial-based therapeutic strategies have garnered significant attention.[4–6] For example, magnetic nanoparticle (MNP)-mediated magnetic hyperthermia,[5,7–10] which utilizes the unique heating property of MNPs under an alternating magnetic field (AMF) to locally heat tumor tissues,[11] has been developed as a prospective modality for cancer treatment.[12–21]

Magnetic hyperthermia can induce cancer cell apoptosis through intracellular magnetic hyperthermia by internalized MNPs or through extracellular magnetic heating by MNP-loaded scaffolds.[3,6,11] Emerging evidences suggest that intracellular magnetic hyperthermia is more efficacious than extracellular magnetic heating in inducing cancer cell apoptosis.[22–25] Intracellular magnetic hyperthermia not only destroys the internal structure of cancer cells more effectively[22,26,27] but also minimizes damage to surrounding healthy tissues.[28,29] However, intracellular magnetic hyperthermia requires the uptake of MNPs by cancer cells. An accelerated cellular uptake of MNPs can increase the therapeutic effect of magnetic hyperthermia.

The cellular uptake of nanomaterials proceeds *via* some pathways such as endocytosis, phagocytosis, micropinocytosis and direct fusion with the cell membrane.[30] Not only cells but also extracellular environment can affect the interaction between cells and nanoparticles and their cellular uptake because cells are surrounded by their extracellular microenvironments.[31] Extracellular microenvironments interact with cells through their specific motifs that bind with their receptors on the cell membranes or through their physical characteristics such as viscoelasticity. Many studies have revealed the influence of the viscoelastic properties of extracellular microenvironments on the adhesion, proliferation, migration and differentiation of cells.[32,33] Substrate stiffness affects the cellular uptake of nanoparticles.[34,35]

Viscosity, as a characteristic property of extracellular microenvironments, varies depending on the type of tissues, health condition and age. The viscosity of the mucus, bone marrow, synovial fluid and interstitial fluid has different values. The viscosity of colorectal cancer (CRC) tissue is significantly higher than that of the normal colorectal tissue due to

[a]*Research Center for Macromolecules and Biomaterials, National Institute for Materials Science, Ibaraki 305-0044, Japan. E-mail: Guoping.CHEN@nims.go.jp*
[b]*Graduate School of Science and Technology, University of Tsukuba, Ibaraki 305-8577, Japan*
[c]*Graduate School of Life and Environmental Science, University of Tsukuba, Ibaraki 305-8572, Japan*

increased mucus production and extracellular matrix remodeling.[36] Recently, some studies have disclosed that the viscosity of the microenvironment can affect stem cell differentiation and anticancer drug resistance of colon cancer cells.[37–41]

Despite increasing interest in nanomaterial-based therapies, it remains unclear how the viscosity of the extracellular microenvironment affects the cellular uptake of MNPs. Elucidating the effect of microenvironmental viscosity on the cellular uptake of MNPs is crucial for the subsequent selection of conditions for magnetic hyperthermia treatment because heat generation and temperature increase during magnetic hyperthermia are correlated with the amount of magnetic nanoparticles in cancer cells. Therefore, the objective of this study is to investigate the influence of viscosity on the cellular uptake of Fe_3O_4 NPs in CRC (SW480) cells (Scheme 1). The cellular uptake of Fe_3O_4 NPs was analyzed and their magnetothermal effect was investigated. Viscosity could inhibit the cellular uptake of NPs and reduce their therapeutic capacity.

2. Materials and methods

2.1. Reagents

Sodium hydroxide (granular), $FeCl_3{\cdot}6H_2O$, $FeCl_2{\cdot}4H_2O$, sodium citrate, polyethylene glycol (PEG) 8M, M_w 8 000 000, PEG 35K, M_w 35 000, DMEM with high glucose and trypsin-EDTA solution (0.25%) were purchased from Sigma-Aldrich, USA. Millipore syringe filter with a 0.45 μm mesh size was purchased from Merck Millipore. The human colorectal cancer cell line SW480 was purchased from the American Type Culture Collection (ATCC, Manassas, VA, USA). Prussian Blue Stain Kit was bought from ScyTek Laboratories, USA. Annexin V-FITC/PI Apoptosis Detection Kit was purchased from MedChemExpress, USA. Ethyl acetate, diethylene glycol (DEG), *N*-methyldiethanolamine (NMDEA), ethanol, 4% Paraformaldehyde Phosphate Buffer Solution (PFA, 4%), bovine serum albumin (BSA), hydrogen peroxide (H_2O_2, 30%) and nitric acid (HNO_3, 67%) were bought from Wako Pure Industries, Ltd.

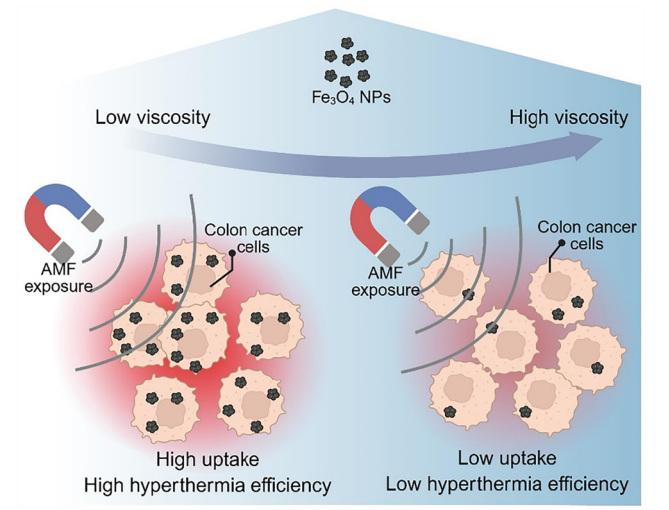

Scheme 1 Influence of viscosity on the cellular uptake of Fe_3O_4 NPs in CRC (SW480) cells and their intracellular magnetic hyperthermia efficiency. The illustration was generated using BioRender (https://app.biorender.com/).

2.2. Synthesis and characterization of Fe_3O_4 NPs

Fe_3O_4 NPs were synthesized *via* a solvothermal method, as described previously.[11,42] Initially, $FeCl_3$ and $FeCl_2$ were mixed in NMDEA and DEG polyols at a molar ratio of 2 : 1 and stirred under a nitrogen atmosphere for 1 h. Subsequently, a sodium hydroxide polyol solution was added dropwise to the ferric chloride mixture and agitated for an additional 3 h. The resulting mixture was then heated to 220 °C, and after 12 h of reaction, a black precipitate was separated using a magnet and washed with an ethanol-ethyl acetate mixture. The separated black precipitate was then dispersed in an aqueous sodium citrate solution and reacted at 60 °C for 24 h to facilitate chelation between NPs and citrate ions. The final citrate-NPs were obtained through centrifugation (12 000 rpm, 15 min) and washed three times with pure water. The morphology and size of the citrate-NPs were examined utilizing a JEOL JEM-ARM200F transmission electron microscope (TEM). Fourier-transform infrared (FT-IR) spectra of the prepared citrate-NPs were recorded. Dynamic light scattering (DLS, Beckman Coulter) was employed to analyze the hydrodynamic size and zeta potential of citrate-NPs in pure water and cell culture media. In addition, in order to evaluate the protein corona formation, scanning electron microscopy (SEM) coupled with energy-dispersive X-ray spectroscopy (EDS) was further utilized to characterize the elemental composition of citrate-NPs before and after incubation in a cell culture medium.

2.3. Preparation of PEG solutions with different viscosities

To regulate the viscosity of cell culture media, two types of PEG were employed: a high-molecular-weight PEG (PEG 8M, M_w 8 000 000) and a low-molecular-weight PEG (PEG 35K, M_w 35 000).[37] The 1.5% (wt/v) PEG stock solution and a 5.75-fold concentrated DMEM with high glucose were individually prepared and sterilized using a Millipore syringe filter (0.45 μm). The complete DMEM with varying viscosities was formulated by combining the PEG solution (1.5% (wt/v)) and concentrated DMEM solution (5.75-fold) at a volume ratio of 4 : 1. This mixture was subsequently supplemented with 1% (v/v) fetal bovine serum (FBS), L-glutamine (584 mg L^{-1}), and antibiotics (100 U mL^{-1} penicillin and 100 μg mL^{-1} streptomycin) to achieve a final concentration of 1-fold DMEM and 1.0% (wt/v) PEG.

The culture media with varying viscosities were prepared by incorporating PEG 35K, PEG 8M, and their combinations at different weight ratios. These groups were named according to their relative viscosity levels as follows: normal viscosity (NV, no PEG); low viscosity (LV, PEG 8M : PEG 35K = 1 : 1); middle viscosity (MV, PEG 8M : PEG 35K = 2 : 1); high viscosity (HV, PEG 8M : PEG 35K = 4 : 1) and very high viscosity (VHV, PEG 8M : PEG 35K = 1 : 0). To prepare media containing Fe_3O_4 NPs, an NP stock solution (10 mg mL^{-1}) was added to the PEG-con-

taining culture media to achieve a final Fe_3O_4 NP concentration of 120 μg mL^{-1}. The mixtures were homogenized by stirring overnight before use.

2.4. Measurement of viscosity

An MCR 302 rheometer (Anton Paar, Germany) was used to determine the viscosity of the culture medium in the rotational shear mode.[37,38] The procedure involved placing 2 mL of the sample on a preheated plate (PP-50) and compressing it with another parallel plate, maintaining a 1.0 mm gap. To prevent evaporation during the measurement, low-viscosity silicone oil was applied to the periphery of the sample. Measurements were conducted at 37 °C with shear rates ranging from 0.1 to 100 s^{-1}. The zero-shear viscosity was defined as the viscosity at a shear rate of 0.1 s^{-1}. For each measurement, three samples were used to calculate the mean and standard deviation.

2.5. Cellular uptake of Fe_3O_4 NPs

SW480 colorectal cancer cells were cultured in DMEM serum supplemented with 1% FBS, L-glutamine, and antibiotics.[37] The cells were maintained in an incubator with controlled humidity at 37 °C and 5% CO_2. Upon reaching approximately 75% confluence, the cells were dissociated and seeded in a 24-well plate at a density of 2.5×10^5 cells per well. After 24 h, a final concentration of 120 μg mL^{-1} of Fe_3O_4 NPs was introduced into the media with different viscosities to investigate the effect of viscosity on the cellular uptake of NPs. Following incubation for different durations (0, 6, 12, 24, 36, and 48 h), the cells were washed five times with PBS to remove non-internalized NPs. The cellular uptake of Fe_3O_4 NPs was monitored *via* Prussian blue staining and quantified by ICP-OES. For Prussian blue staining, the cells were fixed using 4% PFA, and then, the fixed cells were treated with an iron stain solution for 3 min. To provide contrast, cell nuclei were stained with a nuclear fast red solution for 5 min. The stained cells were then examined using an optical microscope in the bright-field mode.

ICP-OES was used to quantify the cellular uptake amount of Fe_3O_4 NPs. SW480 cells were seeded in 24-well plates and incubated for 24 h. Subsequently, the cells were exposed to NPs at a concentration of 120 μg ml^{-1} in various viscous media. Following different incubation periods, the cells were washed five times with PBS to remove non-internalized NPs. The cells were then detached using trypsin/collagenase treatment and collected by centrifugation (1100 rpm, 5 min). The harvested cells were enumerated and subjected to digestion using a mixture of $HNO_3 : H_2O_2$ (1 mL, v/v = 2 : 1). This digested cell solution was subsequently diluted with pure water, filtered and analyzed for iron content using ICP-OES.

2.6. Intracellular pH measurement

The intracellular pH was measured using the pHrodo™ AM variety pack following the manufacturer's protocol. Briefly, the cells were seeded in glass-bottom confocal dishes and allowed to adhere overnight. The culture medium was then exposed to NPs (120 μg ml^{-1}) in various viscous media. After pre-incubation for 24 h under the respective viscosity conditions, cells were incubated with pHrodo™ AM ester diluted in a serum-free medium and incubated for 30 min at 37 °C. After incubation, cells were washed three times with PBS and imaged immediately using a confocal laser scanning microscope.

2.7. Lysosomal trafficking of Fe_3O_4 NPs

To gain deeper mechanistic insights into the intracellular trafficking route of the internalized NPs, rhodamine-labeled Fe_3O_4 NPs (Rho-Fe_3O_4 NPs) were employed in combination with LysoTracker and Hoechst staining for fluorescence imaging, thereby enabling visualization and co-localization of their subcellular distribution within endo/lysosomal compartments. SW480 cells were seeded in plates and then exposed to Rho-Fe_3O_4 NPs (120 μg ml^{-1}) in various viscous media for 24 h. After washing cells with PBS for 5 times, the cells were stained with LysoTracker and Hoechst. The stained cells were then visualized using a fluorescence microscope.

2.8. Magnetic heating performance of intracellular Fe_3O_4 NPs

To investigate the influence of various viscous culture media on the cellular uptake of Fe_3O_4 NPs and the subsequent impact on the magnetic heating effect of intracellular NPs, SW480 cancer cells (5×10^6 cells) were cultured in Petri dishes (P-100, Falcon) using diverse viscous media containing 120 μg mL^{-1} Fe_3O_4 NPs for 24 h. The cells were subsequently washed five times with PBS to remove the non-internalized NPs, resulting in cells containing varying quantities of NPs. These NP-loaded cells were then detached, collected (1100 rpm, 5 min) and resuspended in 100 μL of PBS before being transferred into 0.5 mL Eppendorf tubes. The samples were positioned in the central area of AMF Double H CoilSets and subjected to 10 min irradiation (frequency: 373.6 kHz; field intensity: 130 Oe). During the AMF exposure, the temperature of the cell suspension was recorded utilizing a fiber optic thermometer (Rugged Monitoring, Canada).

To ensure thermal consistency, all heating experiments were conducted in a temperature-controlled environment, using preheated insulation to maintain the ambient temperature at 37 °C ± 0.5 °C, simulating physiological conditions and minimizing the external thermal interference. The baseline temperature before AMF exposure was 37 °C. During irradiation, the temperature of the cell suspension was continuously monitored using a fiber optic thermometer (Rugged Monitoring, Canada), with the probe placed directly in the tube to allow accurate, real-time temperature measurement. Temperature increment was normalized to the cellular uptake amount of Fe_3O_4 NPs by dividing the temperature increment with the respective amount of uptaken Fe_3O_4 NPs.

2.9. Magnetic hyperthermia effect of intracellular Fe_3O_4 NPs

To assess the magnetic hyperthermia effect of different amounts of intracellular Fe_3O_4 NPs, cell apoptosis of SW480 cancer cells was examined following AMF irradiation. Control cells were cultured in DMEM without NPs and PEG. Cells from

the control group and those loaded with various amounts of NPs (as described in section 2.6) were subjected to AMF exposure. Prior to and following AMF irradiation, the cells were suspended in a 1× binding buffer and incubated with Annexin V-FITC conjugate and PI for 10 min in darkness. The stained cell suspensions were filtered through a 35 μm cover and transferred to 12 × 75 mm plastic test tubes. The cell fluorescence was immediately quantified using a flow cytometer (BD Accuri C6 Plus). The viable cells remained unstained by both PI and Annexin V-FITC conjugate. Early apoptotic cells were identified by Annexin V-FITC conjugate staining alone, whereas late apoptotic cells exhibited staining with both Annexin V-FITC conjugate and PI. The apoptosis rate was calculated using both early and late apoptotic cells.

2.10 Statistical analysis

All quantitative experiments were conducted in triplicate (n = 3), and the results are presented as mean ± standard deviation (S.D.). Statistical analysis was performed using one-way analysis of variance (ANOVA). A p value of 0.05 was established as the threshold for statistical significance, with the data categorized as follows: $*p < 0.05$, $**p < 0.01$ and $***p < 0.001$. All analyses were performed using GraphPad Prism 9.0 (GraphPad Software, CA, USA).

3. Results

3.1. Synthesis and characterization of Fe_3O_4 NPs

The Fe_3O_4 NPs were synthesized and modified with citrate to improve the stability of NPs. The morphology of the prepared citrate-NPs was characterized by TEM. As shown in Fig. 1A, the synthesized citrate-Fe_3O_4 NPs displayed a flower-like shape with an average size of 31.4 ± 4.8 nm. FT-IR spectroscopy was employed to verify the citrate modification of NPs. The spectra of bare Fe_3O_4 NPs, citrate-Fe_3O_4 NPs and sodium citrate are illustrated in Fig. 1B. The characteristic absorption peaks at 1384.9 and 1577.8 cm^{-1} are attributed to the symmetric and

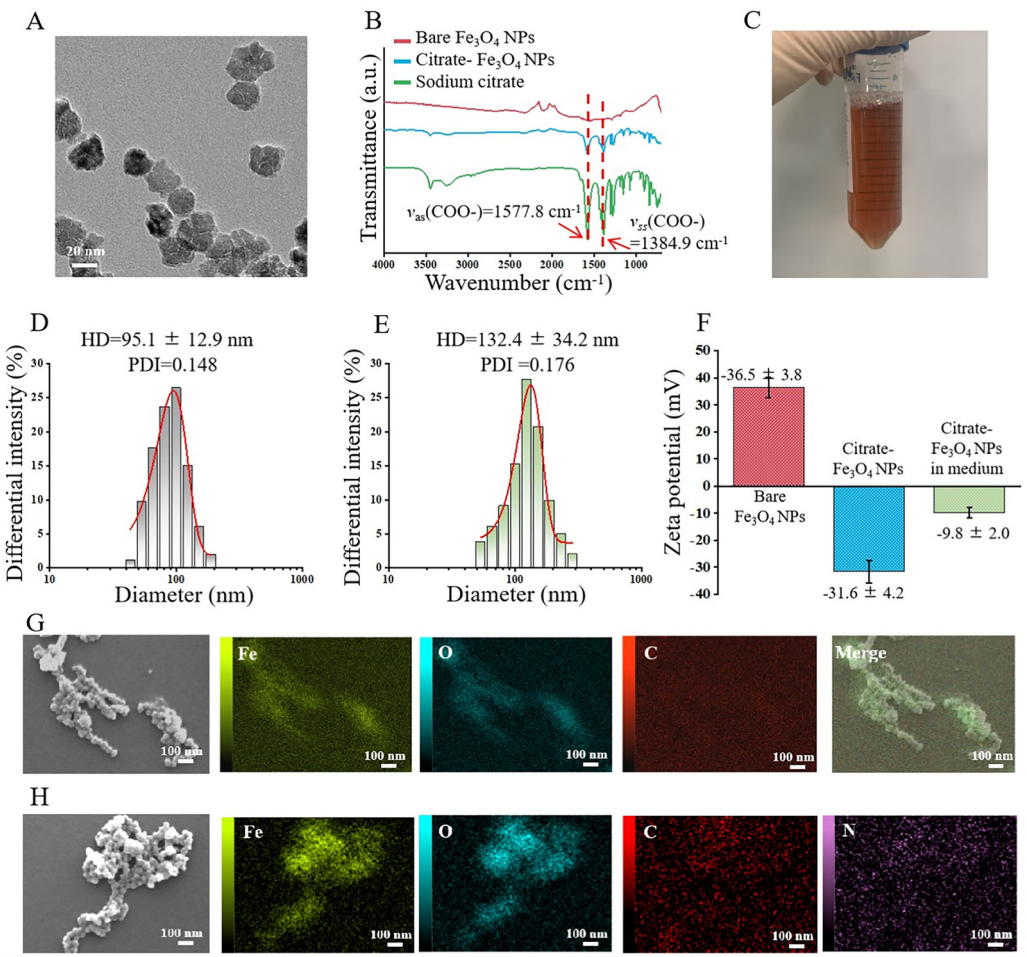

Fig. 1 Characterization of citrate-Fe_3O_4 NPs. (A) TEM images of citrate-Fe_3O_4 NPs (scale bar: 20 nm). (B) FT-IR spectra of bare Fe_3O_4 NPs, citrate-Fe_3O_4 NPs and sodium citrate. (C) Photograph of citrate-Fe_3O_4 NPs in DMEM. (D) Hydrodynamic size distribution of citrate-Fe_3O_4 NPs in pure water. (E) Hydrodynamic size distribution of citrate-Fe_3O_4 NPs in DMEM. (F) Zeta potential of bare-Fe_3O_4 NPs, citrate-Fe_3O_4 NPs and citrate-Fe_3O_4 NPs in DMEM. (G) SEM image with the corresponding elemental mapping of the citrate-Fe_3O_4 NPs. (H) SEM image with the corresponding elemental mapping of the citrate-Fe_3O_4 NPs after incubation in a cell culture medium.

asymmetric stretching vibrations of the COO^- group,[43,44] which are observed in the spectra of sodium citrate and citrate-Fe_3O_4 NPs, but not in the bare Fe_3O_4 NPs. This result revealed the surface modification of Fe_3O_4 NPs with citrate ions, suggesting the successful synthesis of citrate-Fe_3O_4 NPs. The citrate-Fe_3O_4 NPs demonstrated superior dispersion characteristics in the cell culture medium (DMEM), maintaining stability without precipitation (Fig. 1C). The hydrodynamic size and size distribution of citrate-Fe_3O_4 NPs dispersed in water (Fig. 1D) or in DMEM (Fig. 1E) were measured *via* DLS. The hydrodynamic diameters of citrate-Fe_3O_4 NPs were 95.1 ± 12.9 nm in water and 132.4 ± 34.2 nm in DMEM, respectively. The PDI value of the hydrodynamic size of citrate-Fe_3O_4 NPs in pure water and DMEM was 0.148 and 0.174, respectively. In both media, citrate-Fe_3O_4 NPs exhibited a unimodal size distribution, and the relatively small increase in particle size in DMEM indicates that the prepared citrate-Fe_3O_4 NPs maintained good colloidal stability under physiological conditions. Zeta potential analysis revealed a surface charge of +36.5 ± 3.8 mV for bare Fe_3O_4 NPs, which shifted to −31.6 ± 4.2 mV following citrate modification, and further to −9.8 ± 2.1 mV after co-incubation in DMEM (Fig. 1F). The slight enlargement of hydrodynamic size together with the reduction in surface charge in DMEM can be attributed to the adsorption of serum proteins and the consequent formation of a protein corona, which effectively screens the negative surface charge. Moreover, the SEM image and relative elemental mapping of citrate-Fe_3O_4 NPs (Fig. 1G) revealed the co-localization of Fe, O, and C, confirming the presence of a citrate coating. In addition, the appearance of N after the incubation of citrate-Fe_3O_4 NPs in a cell culture medium (Fig. 1H) demonstrated the formation of protein corona. These results suggested that while the formation of a protein corona alters the interfacial properties of the NPs, it does not compromise their colloidal stability, thereby ensuring reliable performance under biologically relevant conditions. The citrate-Fe_3O_4 NPs were used for cell culture to investigate the influence of viscosity of culture media on their uptake.

3.2. Preparation and characterization of cell culture media of different viscosities

The cell culture media with various viscosities were prepared by adding the same amount but different ratios of low-molecular-weight PEG 35K and high-molecular-weight PEG 8M in the culture media. A rheometer was utilized to assess the viscosity of cell culture media at 37 °C, employing shear rates ranging from 0.1 to 100 s^{-1}. The results (Fig. 2A) demonstrated that the medium's viscosity decreased with the increasing shear rate. Furthermore, the viscosity value at a shear rate of 0.1 s^{-1} was determined as the zero-shear viscosity[39] and the zero-shear viscosity (Fig. 2B) of the culture media exhibited an increase as the proportion of PEG 8M increased. The viscosity of the culture medium was modulated within a range of 32.6 ± 1.86 to 619.8 ± 70.4 mPa s (Table 1) by altering the weight ratio of PEG 8M and PEG 35K, encompassing a viscosity range characteristic of the mucus layer.[45]

3.3. Prussian blue staining and quantification of internalized Fe_3O_4 NPs

The internalization of Fe_3O_4 NPs by cells during the cultivation process was visualized *via* Prussian blue staining. SW480 colon cancer cells were cultured in culture media of various viscosities containing 120 μg mL^{-1} NPs for a duration of 0–48 h. The results of Prussian blue staining (Fig. 3) demonstrated that although the cells were capable of internalizing NPs in media of different viscosities, large differences among the cells cultured in media of different viscosities during uptake were observed. In the control group, medium without PEG (PEG 8M : 35K = 0 : 0), the uptake of Fe_3O_4 NPs by the cells increased gradually during the initial 12 h of culture. However, as the incubation time was extended to 48 h, a slight decrease in Fe_3O_4 NPs uptake was observed, potentially due to cell division and metabolic processes. In contrast, the uptake of NPs by cells was reduced in the PEG-containing media.

This phenomenon might be attributed to the effect of increased medium viscosity on the diffusion behavior of NPs.[46]

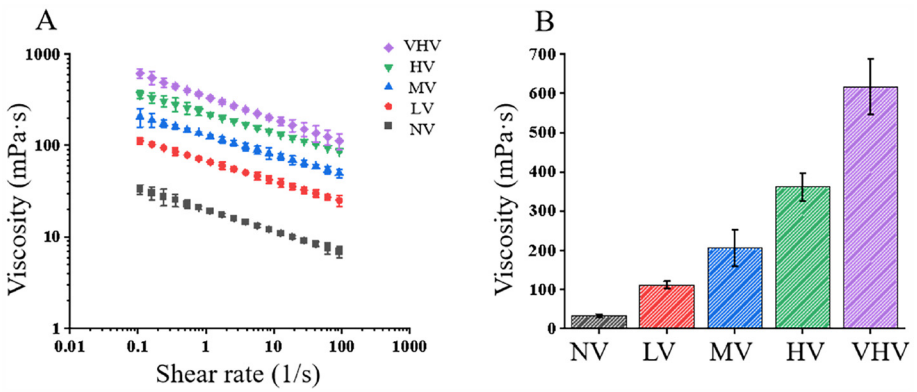

Fig. 2 Characterization of the viscosity of cell culture media containing different ratios of PEG 35K and PEG 8M. (A) Steady shear rate measurement of apparent viscosity of cell culture media ranging from 0.1 to 100 s^{-1} at 37 °C. (B) Zero-shear viscosity of cell culture media measured at a shear rate of 0.1 s^{-1}.

Table 1 Zero-shear viscosity of cell culture media with varying PEG weight ratios measured at a shear rate of 0.1 s^{-1}

Sample	NV	LV	MV	HV	VHV
Viscosity (mPa s)	32.6 ± 1.86	112.7 ± 9.0	205.4 ± 46.8	362.0 ± 35.5	619.8 ± 70.4

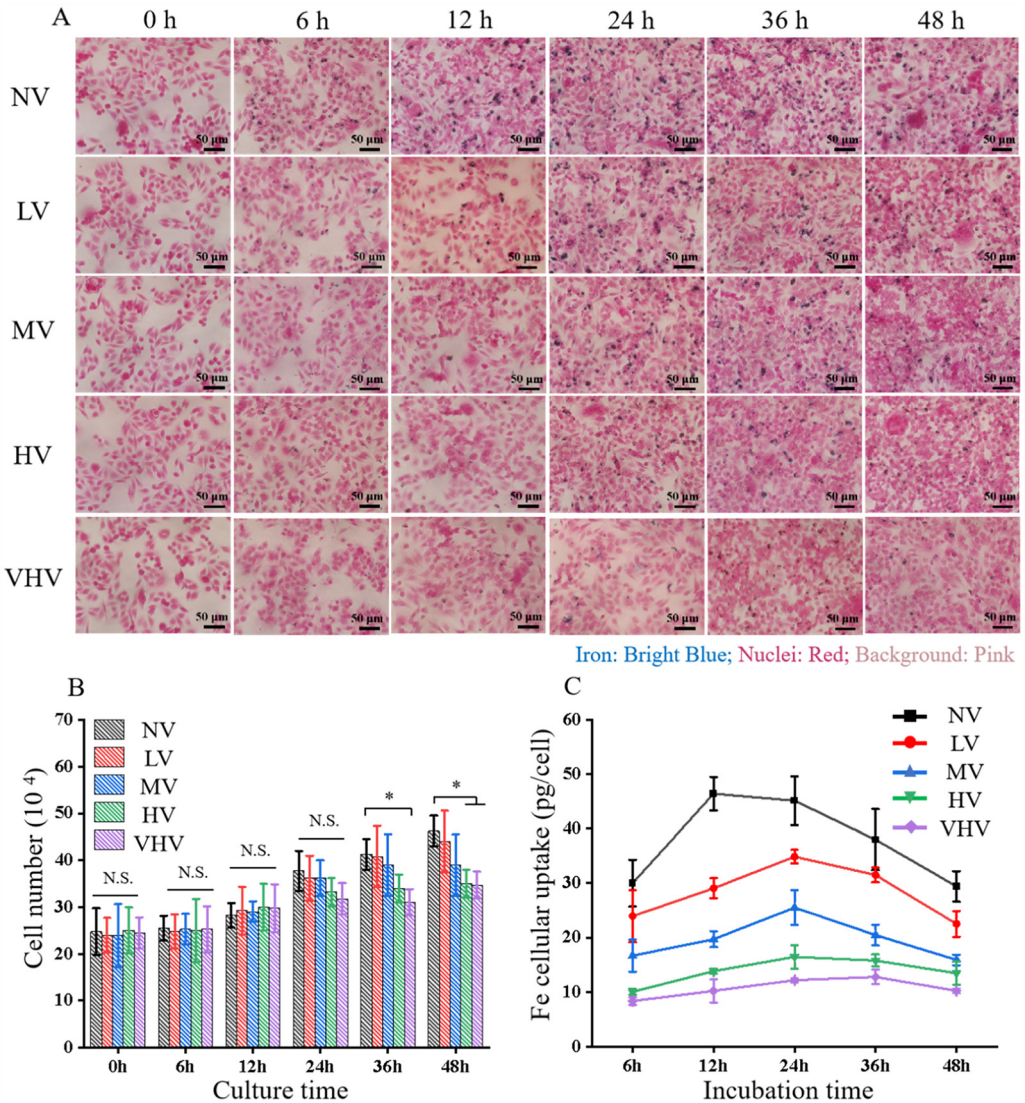

Fig. 3 Internalization and quantification of Fe_3O_4 NPs in SW480 cells cultured in media of different viscosities. (A) Prussian blue staining of the internalized Fe_3O_4 NPs in SW480 cells cultured in media of different viscosities in the presence of 120 μg mL^{-1} Fe_3O_4 NPs for 0, 6, 12, 24, 36 and 48 h. Change in the (B) cell number and (C) cellular uptake amount of Fe_3O_4 NPs during culture in different viscosity media in the presence of 120 μg mL^{-1} Fe_3O_4 NPs for 0, 6, 12, 24, 36 and 48 h. Data are expressed as mean ± S.D. (n = 3). Significant difference: *p < 0.05. N.S.: no significant difference.

Higher viscosity restricts the ability of NPs to diffuse in the medium, thereby reducing their probability of reaching the cell surface and consequently inhibiting the internalization efficiency.[35] Furthermore, the high viscous microenvironment may affect the fluidity and deformability of cell membranes,[47–49] further inhibiting the uptake of NPs. Notably, the uptake of Fe_3O_4 NPs by cells exhibited a decreasing trend with the increasing medium viscosity, further suggesting that the rheological property of the extracellular microenvironment plays a crucial role in regulating the cellular uptake of NPs.

The cellular uptake of Fe_3O_4 NPs was quantified by ICP-OES after the cells were cultured in media of different viscosities in the presence of 120 μg mL^{-1} Fe_3O_4 NPs for 6, 12, 24, 36 and 48 h. During cell culture, the cells proliferated and cell number changed. To calculate the average amount of internalized Fe_3O_4 NPs per cell, the cell number was first measured

(Fig. 3B). The cell number increased with culture time. The cell number increased more slowly in the high-viscosity medium than did in the low viscosity medium.

The ICP-OES quantification results (Fig. 3C) revealed that the cellular uptake of NPs in all groups initially increased and subsequently decreased with culture time. Additionally, the culture medium viscosity significantly influenced the cellular uptake of NPs, with the increased viscosity resulting in decreased cellular uptake of NPs. In a culture medium without PEG (PEG 8M : PEG 35K = 0 : 0), the intracellular amounts of NPs reached the maximum at 12 h. In a culture medium with PEG 8M : PEG 35K ratios of 1 : 1, 2 : 1 and 3 : 1, the cellular uptake amounts of NPs peaked at 24 h. In the PEG 8M : PEG 35K = 4 : 1 group, the peak of NP uptake was delayed until 36 h. The results indicated that the viscosity of the medium could slow down and suppress the cellular uptake of Fe_3O_4 NPs.

3.4. Intracellular pH measurements

To determine whether the changes in extracellular viscosity alter intracellular acidification, the intracellular pH under different viscosity conditions using the pHrodo™ AM indicator was measured. As shown in Fig. 4, no significant difference in fluorescence intensity was observed among the tested groups, indicating that the intracellular pH remained stable despite variations in environmental viscosity. These results demonstrate that the viscosity modulation does not disrupt intracellular pH homeostasis, and therefore, is unlikely to interfere with Fe_3O_4 NP degradation and magnetothermal activity.

3.5. Lysosomal trafficking of Fe_3O_4 NPs

The above Prussian blue staining and ICP quantification (Fig. 3) results demonstrated that the medium viscosity strongly influenced the overall uptake efficiency, and these observations alone could not reveal the subsequent intracellular fate of the NPs. To further elucidate the intracellular trafficking pathway of the internalized NPs, Rho-Fe_3O_4 NPs were employed in combination with LysoTracker and Hoechst staining to visualize their subcellular localization. Therefore, fluorescence co-localization analysis was used to investigate whether the internalized NPs were delivered to lysosomes, the major destination of endocytic vesicles. The merged fluorescence images confirmed the co-localization of Rho-Fe_3O_4 NPs with LysoTracker-stained lysosomes (Fig. 5), indicating that the cellular internalization of Fe_3O_4 NPs predominantly occurs through the endo-lysosomal pathway. Importantly, this lysosomal trafficking pattern remained unchanged across media of different viscosities, suggesting that although extracellular rheological conditions regulate the efficiency of NP uptake, they do not alter the fundamental intracellular internalization route.

3.6. Magnetic heating effect of intracellular Fe_3O_4 NPs

Based on the results shown in Fig. 3B and C, the cells cultured in different viscosity media containing 120 μg mL^{-1} Fe_3O_4 NPs for 24 h were used for investigating magnetic heating effect. The results in Fig. 6A and B revealed that cells without NPs (control) did not induce temperature increase, while different amounts of intracellular NPs resulted in varying degrees of temperature changes. The cells cultured without PEG exhibited the highest uptake of NPs (Fig. 6B) and consequently caused the most significant temperature change, with a temperature rise of 7.3 ± 0.5 °C. This was followed by the group cultured in the viscous medium prepared by adding PEG 8M and PEG 35K at a ratio of 1 : 1, in which the intracellular NPs led to a temperature increase of 5.4 ± 0.7 °C. When PEG 8M : PEG 35K = 1 : 0 were added in the culture medium, the cells were exposed to the highest viscosity and internalized the least amounts of Fe_3O_4 NPs, resulting in an increase in temperature of only 2.3 ± 0.3 °C. When the temperature increment was normalized to the cellular uptake amount of Fe_3O_4 NPs, the temperature increment per amount of uptaken Fe_3O_4 NPs was not significantly different among the 5 samples (Fig. 6C). The results indicated that the temperature increment was predominantly due to the uptake amount of Fe_3O_4 NPs.

3.7. Magnetic hyperthermia effect of internalized Fe_3O_4 NPs

When the temperature slightly exceeds the normal physiological limit, it can cause proteins to unfold, become entangled and form non-specific clumps.[50] This can trigger the heat shock response and lead to the onset of programmed cell death.[51,52] The various temperature increments generated by different intracellular amounts of NPs might induce different degrees of cell apoptosis. Therefore, cell apoptosis was analyzed before and after AMF irradiation, and the results are shown in Fig. 7A and B.

Cells cultured in a normal medium without Fe_3O_4 NPs and PEG were used as a control. Before AMF irradiation, there was no significant difference in cell apoptosis compared to cells in the control group, indicating that PEG and NPs could not induce cell apoptosis. However, after AMF irradiation, the apoptotic rate of cells cultured in the normal medium without PEG significantly increased to 40.2% ± 4.8% compared to the control group. Moreover, with the increase in the viscosity of

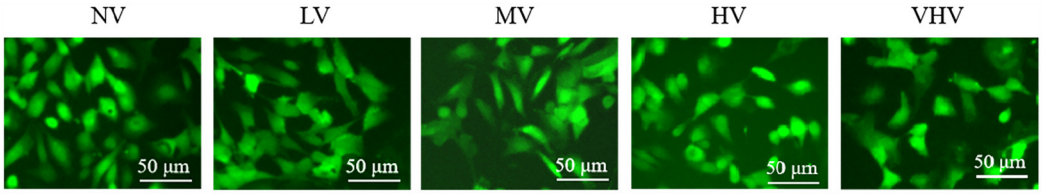

Fig. 4 Intracellular pH measurements under different viscosity media using the pHrodo™ AM assay.

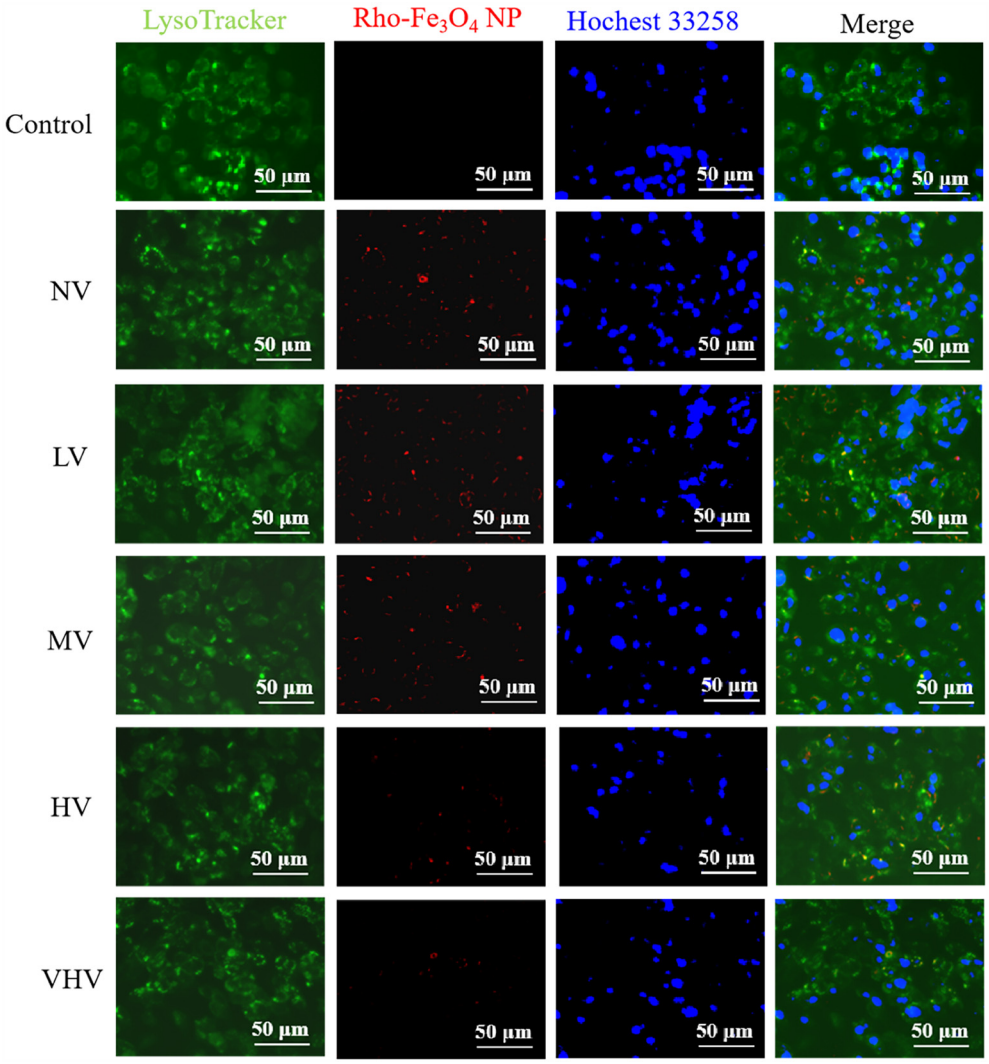

Fig. 5 Fluorescence imaging of SW480 cells incubated with Rho-Fe_3O_4 NPs (red) under media of different viscosities, co-stained with Lyso Tracker (green) to visualize lysosomes and Hoechst 33258 (blue) for nuclear staining.

cell culture medium by adjusting the weight ratio of PEG 8M and PEG 35K from 1 : 1 (LV) to 1 : 0 (VHV), the cell apoptotic rate gradually decreased from 22.8% ± 2.2% to 9.45% ± 0.7% because the various viscosities of culture media influenced the NPs internalization and further influenced the magnetic hyperthermia effect.

4. Discussion

In this study, the influences of microenvironmental viscosity on the uptake of Fe_3O_4 NPs by CRC cells and the intracellular magnetic hyperthermia were investigated. The results demonstrated that both the uptake rate and the uptake amount of Fe_3O_4 NPs decreased significantly with the increasing microenvironmental viscosity, which led to the limitation of intracellular magnetic hyperthermia and ultimately reduced the apoptosis rate. These findings suggest that the viscosity of microenvironment could regulate Fe_3O_4 NP uptake and the efficacy of magnetothermal therapy.

The influence of viscosity on the cellular uptake of Fe_3O_4 NPs may be explained through its dual effect on Fe_3O_4 NP diffusion and cell membrane dynamics. The diffusion of NPs in the cellular microenvironment can be influenced by a variety of physicochemical factors, among which the solution viscosity is an important regulatory parameter. According to the Stokes–Einstein equation,[53] the diffusion coefficient is inversely related to the solution viscosity, and thus, the diffusion of Fe_3O_4 NPs is limited in a high viscosity microenvironment, resulting in a reduced chance of them to reach the cell membrane. In addition, the high viscosity may reduce the fluidity of the cell membrane, thereby affecting the distribution and function of endocytosis-associated receptors and further inhibiting receptor-mediated endocytosis and other NP uptake pathways.[47–49]

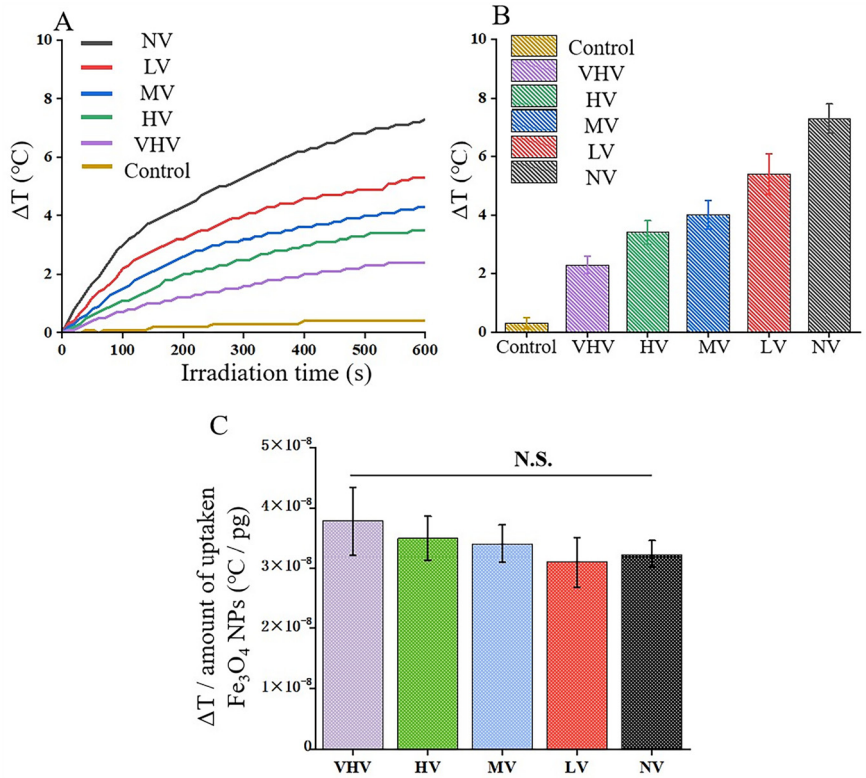

Fig. 6 Magnetic heating effect of internalized Fe_3O_4 NPs. (A) Temperature–time curve of internalized Fe_3O_4 NPs during AMF exposure. (B) Temperature increment after 10 min of AMF exposure. (C) Temperature increment normalized to uptake amount of Fe_3O_4 NPs. Data are expressed as mean ± S.D. (n = 3). N.S.: no significant difference.

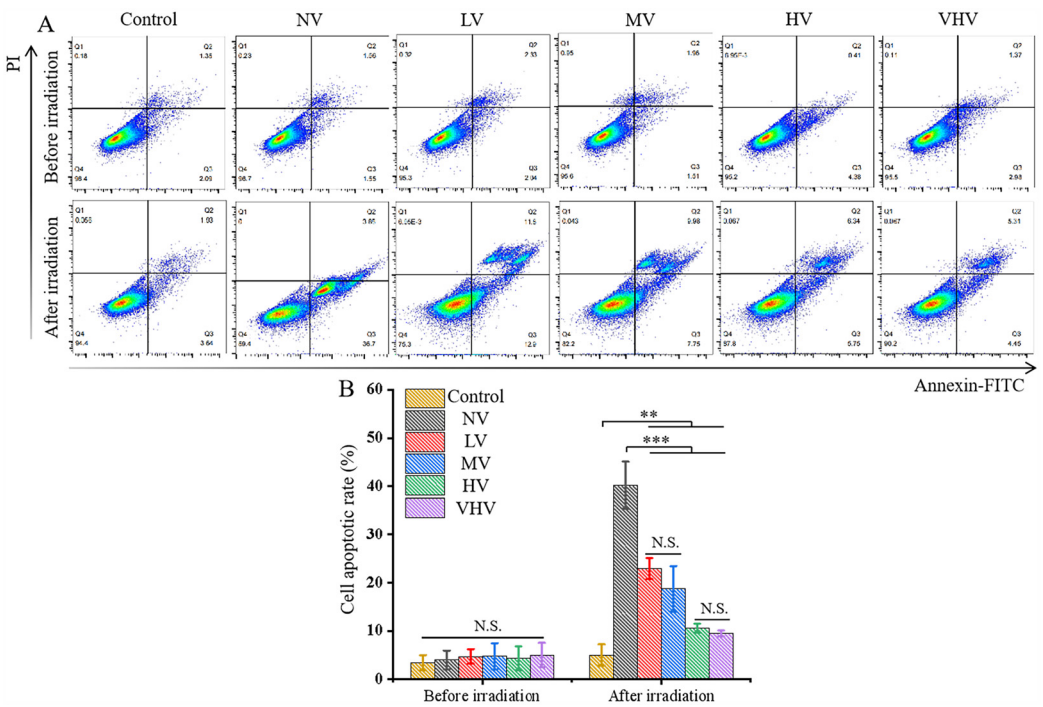

Fig. 7 Apoptosis of SW480 cells induced by intracellular magnetic hyperthermia of internalized Fe_3O_4 NPs. (A) Representative flow cytometry image and (B) apoptosis rate of SW480 cells with different intracellular amounts of NPs after AMF irradiation. Data are expressed as mean ± S.D. (n = 3). Significant difference: $^{**}p < 0.01$, $^{***}p < 0.001$. N.S.: no significant difference.

The observed differences in magnetic hyperthermia performance are attributed to variations in the internalized Fe_3O_4 NPs when the cells were cultured in different viscosity media. A larger amount of internalized Fe_3O_4 NPs could generate more heat to reach a higher temperature and induce a high ratio of apoptosis because the magnetothermal property of Fe_3O_4 NPs is correlated with the amounts of NPs. In a high-viscosity microenvironment, the magnetic heating effect was weakened due to the decreased intracellular uptake amount of Fe_3O_4 NPs, resulting in a decreased apoptosis rate. This phenomenon suggests that the microenvironmental viscosity could affect the magnetic hyperthermia efficiency through its influence on the cellular uptake of Fe_3O_4 NPs. Therefore, the microenvironmental viscosity of tumor tissues should be considered when designing MNP-based magnetothermal therapy protocols to optimize the therapeutic effects.

In addition to viscosity, various physicochemical and biological factors are known to affect the cellular nanoparticle uptake, such as particle size, surface charge, protein corona formation, nanoparticle surface chemistry, cell type, and incubation conditions. In this study, the Fe_3O_4 NPs were coated with citrate, which provides good colloidal stability and a negatively charged surface, facilitating reproducible cellular interactions under different medium conditions. Although the intracellular pH may also influence nanoparticle trafficking, the present study focused primarily on extracellular viscosity; under standard culture conditions, pH variations are expected to be limited and not anticipated to significantly affect the Fe_3O_4 NP uptake.

In summary, the present study demonstrated that microenvironmental viscosity is an important factor in affecting Fe_3O_4 NP uptake and intracellular magnetothermal efficacy. A highly viscous microenvironment could limit the diffusion of Fe_3O_4 NPs and inhibit cellular uptake, thus reducing the heating effect and apoptosis rate of magnetic hyperthermia. These findings provide some useful information for the optimization of CRC magnetothermal therapy and help to guide the design of nanomedicine-based strategies to improve the therapeutic efficacy of magnetic hyperthermia.

5. Conclusion

In this study, the viscosity of cell culture media was modulated by PEG of different molecular weights to simulate the viscous microenvironments of colorectal cancer for the investigation of microenvironmental viscosity effect on the cellular uptake of Fe_3O_4 NPs and intracellular magnetic hyperthermia. The results showed that the uptake speed and amount of Fe_3O_4 NPs by CRC cells decreased with the increase in microenvironmental viscosity, which led to a decrease in intracellular magnetic hyperthermia. The killing effect of magnetic hyperthermia was reduced and the apoptosis rate was significantly decreased in a high-viscosity microenvironment due to the decreased amounts of internalized NPs. The results of this study provide some new insights into the role of viscosity of the CRC tissue microenvironment in the regulation of NP uptake and magnetic hyperthermia.

Author contributions

Conceptualization: G. C., M. W., Y. Y.; funding acquisition: G. C., N. K.; project administration: G. C.; resources: G. C.; supervision: G. C.; date curation: G. C., M. W., N. K.; formal analysis: G. C., M. W., H. C., T. Y.; investigation: G. C., M. W., T. Z., C. L., R. S., H. C., T. Y.; methodology: G. C., M. W., T. Z., C. L., H. C., R. S., T. Y., N. K., Y. Y.; validation: G. C., M. W., N. K.; software: M. W., N. K.; visualization: M. W.; writing – original draft: all authors; writing – review and editing: all authors.

Conflicts of interest

The authors declare no competing interests.

Data availability

The data that support the findings of this study are available from the corresponding author on request.

Acknowledgements

This research was supported by JSPS KAKENHI Grant Numbers 22K19926 and 24K03289.

References

1 Z. Cheng, M. Li, R. Dey and Y. Chen, *J. Hematol. Oncol.*, 2021, **14**, 85.
2 J. Mohapatra, S. Nigam, J. George, A. C. Arellano, P. Wang and J. P. Liu, *Mater. Today Phys.*, 2023, **32**, 101003.
3 M. Wang, R. Sun, H. Chen, T. Yoshitomi, H. Mamiya, M. Takeguchi, N. Kawazoe, Y. Yang and G. Chen, *Mater. Horiz.*, 2025, **12**, 4363–4378.
4 J. Wang, W. Zhao, Z. Zhang, X. Liu, T. Xie, L. Wang, Y. Xue and Y. Zhang, *Adv. Mater.*, 2024, **36**, 2308915.
5 P. Chandrasekharan, Z. W. Tay, D. Hensley, X. Y. Zhou, B. K. Fung, C. Colson, Y. Lu, B. D. Fellows, Q. Huynh, C. Saayujya, E. Yu, R. Orendorff, B. Zheng, P. Goodwill, C. Rinaldi and S. Conolly, *Theranostics*, 2020, **10**, 2965–2981.
6 R. Sun, M. Wang, T. Zeng, H. Chen, T. Yoshitomi, M. Takeguchi, N. Kawazoe, Y. Yang and G. Chen, *Bioact. Mater.*, 2025, **44**, 205–219.
7 S. Shen, J.-X. Xia and J. Wang, *Biomaterials*, 2016, **74**, 1–18.
8 A. Andreozzi, L. Brunese, A. Cafarchio, P. Netti and G. P. Vanoli, *Int. J. Therm. Sci.*, 2025, **208**, 109428.

9 L. Chen, Y. Wu, H. Wu, J. Li, J. Xie, F. Zang, M. Ma, N. Gu and Y. Zhang, *Acta Biomater.*, 2019, **96**, 491–504.
10 X. Liu, Y. Zhang, Y. Wang, W. Zhu, G. Li, X. Ma, Y. Zhang, S. Chen, S. Tiwari, K. Shi, S. Zhang, H. M. Fan, Y. X. Zhao and X.-J. Liang, *Theranostics*, 2020, **10**, 3793–3815.
11 R. Sun, H. Chen, M. Wang, T. Yoshitomi, M. Takeguchi, N. Kawazoe, Y. Yang and G. Chen, *Biomaterials*, 2024, **307**, 122511.
12 E. Bertuit, E. Benassai, G. Mériguet, J.-M. Greneche, B. Baptiste, S. Neveu, C. Wilhelm and A. Abou-Hassan, *ACS Nano*, 2022, **16**, 271–284.
13 V. F. Cardoso, A. Francesko, C. Ribeiro, M. Bañobre-López, P. Martins and S. Lanceros-Mendez, *Adv. Healthcare Mater.*, 2018, **7**, 1700845.
14 M. Ognjanović, D. M. Stanković, Ž. K. Jaćimović, M. Kosović-Perutović, B. Dojčinović and B. Antić, *J. Alloys Compd.*, 2021, **884**, 161075.
15 M. Ayubi, M. Karimi, S. Abdpour, K. Rostamizadeh, M. Parsa, M. Zamani and A. Saedi, *Mater. Sci. Eng., C*, 2019, **104**, 109810.
16 A. Chiu-Lam and C. Rinaldi, *Adv. Funct. Mater.*, 2016, **26**, 3933–3941.
17 H. Gavilán, S. K. Avugadda, T. Fernández-Cabada, N. Soni, M. Cassani, B. T. Mai, R. Chantrell and T. Pellegrino, *Chem. Soc. Rev.*, 2021, **50**, 11614–11667.
18 R. Hergt, S. Dutz and M. Röder, *J. Phys.: Condens. Matter*, 2008, **20**, 385214.
19 D. Caruntu, G. Caruntu, Y. Chen, C. J. O'Connor, G. Goloverda and V. L. Kolesnichenko, *Chem. Mater.*, 2004, **16**, 5527–5534.
20 H. Gavilán, K. Simeonidis, E. Myrovali, E. Mazarío, O. Chubykalo-Fesenko, R. Chantrell, Ll. Balcells, M. Angelakeris, M. P. Morales and D. Serantes, *Nanoscale*, 2021, **13**, 15631–15646.
21 S. Tong, C. A. Quinto, L. Zhang, P. Mohindra and G. Bao, *ACS Nano*, 2017, **11**, 6808–6816.
22 L. Beola, L. Asín, C. Roma-Rodrigues, Y. Fernández-Afonso, R. M. Fratila, D. Serantes, S. Ruta, R. W. Chantrell, A. R. Fernandes, P. V. Baptista, J. M. De La Fuente, V. Grazú and L. Gutiérrez, *ACS Appl. Mater. Interfaces*, 2020, **12**, 43474–43487.
23 Y. Gu, R. Piñol, R. Moreno-Loshuertos, C. D. S. Brites, J. Zeler, A. Martínez, G. Maurin-Pasturel, P. Fernández-Silva, J. Marco-Brualla, P. Téllez, R. Cases, R. N. Belsué, D. Bonvin, L. D. Carlos and A. Millán, *ACS Nano*, 2023, **17**, 6822–6832.
24 X. Wang, J. Law, M. Luo, Z. Gong, J. Yu, W. Tang, Z. Zhang, X. Mei, Z. Huang, L. You and Y. Sun, *ACS Nano*, 2020, **14**, 3805–3821.
25 M. Wang, H. Chen, R. Sun, T. Zeng, C. Lu, T. Yoshitomi, H. Mamiya, M. Takeguchi, N. Kawazoe, Y. Yang and G. Chen, *Acta Biomater.*, 2025, **205**, 634–647.
26 N. Daviu, Y. Portilla, M. Gómez De Cedrón, A. Ramírez De Molina and D. F. Barber, *Biomaterials*, 2024, **304**, 122409.
27 X. Liu, J. Zheng, W. Sun, X. Zhao, Y. Li, N. Gong, Y. Wang, X. Ma, T. Zhang, L.-Y. Zhao, Y. Hou, Z. Wu, Y. Du, H. Fan, J. Tian and X.-J. Liang, *ACS Nano*, 2019, **13**, 8811–8825.
28 S. K. Sharma, N. Shrivastava, F. Rossi, L. D. Tung and N. T. K. Thanh, *Nano Today*, 2019, **29**, 100795.
29 W. Chen, G. Luo and X. Zhang, *Adv. Mater.*, 2019, **31**, 1802725.
30 J. Li, H. Mao, N. Kawazoe and G. Chen, *Biomater. Sci.*, 2017, **5**, 173–189.
31 A. B. Engin, D. Nikitovic, M. Neagu, P. Henrich-Noack, A. O. Docea, M. I. Shtilman, K. Golokhvast and A. M. Tsatsakis, *Part. Fibre Toxicol.*, 2017, **14**, 22.
32 C. Lu, J. Zheng, T. Yoshitomi, N. Kawazoe, Y. Yang and G. Chen, *ACS Appl. Bio Mater.*, 2023, **6**, 3441–3450.
33 X. Wang, Y. Yang, Y. Wang, C. Lu, X. Hu, N. Kawazoe, Y. Yang and G. Chen, *Acta Biomater.*, 2024, **182**, 81–92.
34 C. Huang, P. J. Butler, S. Tong, H. S. Muddana, G. Bao and S. Zhang, *Nano Lett.*, 2013, **13**, 1611–1615.
35 C. M. Beddoes, C. P. Case and W. H. Briscoe, *Adv. Colloid Interface Sci.*, 2015, **218**, 48–68.
36 R. L. Maywald, S. K. Doerner, L. Pastorelli, C. De Salvo, S. M. Benton, E. P. Dawson, D. G. Lanza, N. A. Berger, S. D. Markowitz, H.-J. Lenz, J. H. Nadeau, T. T. Pizarro and J. D. Heaney, *Proc. Natl. Acad. Sci. U. S. A.*, 2015, **112**, DOI: 10.1073/pnas.1422445112.
37 T. Zeng, C. Lu, M. Wang, H. Chen, T. Yoshitomi, N. Kawazoe, Y. Yang and G. Chen, *J. Mater. Chem. B*, 2025, **13**, 2180–2191.
38 C. Lu, T. Zeng, M. Wang, T. Yoshitomi, N. Kawazoe, Y. Yang and G. Chen, *Biomater. Sci.*, 2024, **12**, 5598–5609.
39 J. Zheng, H. Chen, C. Lu, T. Yoshitomi, N. Kawazoe, Y. Yang and G. Chen, *J. Mater. Chem. B*, 2023, **11**, 7424–7434.
40 K. Lee, Y. Chen, X. Li, N. Kawazoe, Y. Yang and G. Chen, *J. Mater. Sci. Technol.*, 2021, **63**, 1–8.
41 K. Lee, Y. Chen, T. Yoshitomi, N. Kawazoe, Y. Yang and G. Chen, *Adv. Healthcare Mater.*, 2020, **9**, 2000617.
42 M. Wang, R. Sun, H. Chen, X. Liu, T. Yoshitomi, M. Takeguchi, N. Kawazoe, Y. Yang and G. Chen, *Microstructures*, 2023, **3**, 2023042.
43 R. Sun, H. Chen, J. Zheng, T. Yoshitomi, N. Kawazoe, Y. Yang and G. Chen, *Adv. Healthcare Mater.*, 2023, **12**, 2202604.
44 M. A. Dheyab, A. A. Aziz, M. S. Jameel, O. A. Noqta, P. M. Khaniabadi and B. Mehrdel, *Sci. Rep.*, 2020, **10**, 10793.
45 M. A. Miller and S. Medina, *Adv. Funct. Mater.*, 2024, **34**, 2402514.
46 Q. Xu, N. J. Boylan, J. S. Suk, Y.-Y. Wang, E. A. Nance, J.-C. Yang, P. J. McDonnell, R. A. Cone, E. J. Duh and J. Hanes, *J. Controlled Release*, 2013, **167**, 76–84.
47 L. Beney and P. Gervais, *Appl. Microbiol. Biotechnol.*, 2001, **57**, 34–42.
48 J. Steinkühler, E. Sezgin, I. Urbančič, C. Eggeling and R. Dimova, *Commun. Biol.*, 2019, **2**, 337.

49 M. Moros, B. Hernáez, E. Garet, J. T. Dias, B. Sáez, V. Grazú, Á. González-Fernández, C. Alonso and J. M. De La Fuente, *ACS Nano*, 2012, **6**, 1565–1577.
50 G. Wei, Z. Su, N. P. Reynolds, P. Arosio, I. W. Hamley, E. Gazit and R. Mezzenga, *Chem. Soc. Rev.*, 2017, **46**, 4661–4708.
51 W.-S. Liu, Z. Chen, Z.-M. Lu, J.-H. Dong, J.-H. Wu, J. Gao, D. Deng and M. Li, *J. Controlled Release*, 2024, **371**, 406–428.
52 P. V. Londhe, M. V. Londhe, A. B. Salunkhe, S. S. Laha, O. T. Mefford, N. D. Thorat and V. M. Khot, *Coord. Chem. Rev.*, 2025, **522**, 216228.
53 A. Baer, S. E. Wawra, K. Bielmeier, M. J. Uttinger, D. M. Smith, W. Peukert, J. Walter and A. Smith, *Small*, 2024, **20**, 2304670.